ACS Chemical Neuroscience

Research Article

pubs.acs.org/chemneuro

Effect of the English Familial Disease Mutation (H6R) on the Monomers and Dimers of Aβ40 and Aβ42

Man Hoang Viet,*[,†] Phuong H. Nguyen,*[,‡] Philippe Derreumaux,*[,§,∥] and Mai Suan Li*[,†,⊥]

[†]Institute of Physics, Polish Academy of Sciences, Al. Lotnikow 32/46, 02-668 Warsaw, Poland

[‡]Laboratoire de Biochimie Theorique, UPR 9080 CNRS, IBPC, Universite Paris 7, 13 rue Pierre et Marie Curie, 75005 Paris, France

[§]Laboratoire de Biochimie Theorique, UPR 9080 CNRS, IBPC, Universite Denis Diderot, Paris Sorbonne Cité 13 rue Pierre et Marie Curie, 75005 Paris, France

[∥]Institut Universitaire de France, Bvd Saint Michel, 75005 Paris, France

[⊥]Institute for Computational Science and Technology, Quang Trung Software City, Tan Chanh Hiep Ward, District 12, Ho Chi Minh City, Vietnam

Supporting Information

ABSTRACT: The self-assembly of the amyloid beta (Aβ) peptides into senile plaques is the hallmark of Alzheimer's disease. Recent experiments have shown that the English familial disease mutation (H6R) speeds up the fibril formation process of alloforms $Aβ_{40}$ and $Aβ_{42}$ peptides altering their toxicity to cells. We used all-atom molecular dynamics simulations at microsecond time scales with the OPLS-AA force field and TIP4P explicit water model to study the structural dynamics of the monomer and dimer of H6R sequences of both peptides. The reason behind the self-assembly acceleration is common that upon mutation the net charge is reduced leading to the weaker repulsive interaction between chains that facilitates the peptide association. In addition, our estimation of the solvation free energy shows that the mutation enhances the hydrophobicity of both peptides speeding up their aggregation. However, we can show that the acceleration mechanisms are different for different peptides: the rate of fibril formation of $Aβ_{42}$ increases due to increased β-structure at the C-terminal in both monomer and dimer and enhanced stability of salt bridge Asp23-Lys28 in monomer, while the enhancement of turn at residues 25−29 and reduction of coil in regions 10−13, 26−19, and 30−34 would play the key role for $Aβ_{40}$. Overall, our study provides a detailed atomistic picture of the H6R-mediated conformational changes that are consistent with the experimental findings and highlights the important role of the N-terminal in Aβ peptide aggregation.

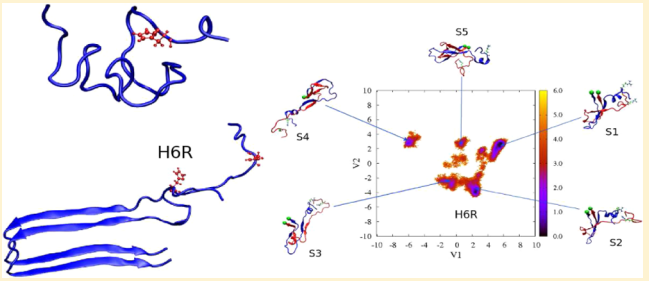

KEYWORDS: *Amyloid simulations, Alzheimer's disease, amyloid-β proteins, molecular dynamics, H6R mutation, monomer, dimer*

Alzheimer's disease (AD) is a type of dementia that causes problems with memory, thinking, and behavior mainly among the senior population.[1] The etiology of AD is complex, but the prominent amyloid cascade hypothesis posits that the deposition of the amyloid beta (Aβ) peptide in the brain parenchyma is a crucial step that ultimately leads to AD.[2−4] Evidence accumulated during last years shows that neither mature fibrils nor monomers of Aβ peptides are toxic but the aesthetic of the cerebral defects in AD rather correlates with high levels of oligomers in the brain.[5,6] This leads to the strategy to cope with AD that is based on preventing or reversing formation of toxic oligomers.[2,3,7−15]

It is well-known that mutations can alter the toxicity, assembly, and rate of fibril formation of Aβ peptides. Since the turn region 21−23 of Aβ peptides might play a crucial step in fibril formation, numerous experimental[16−21] as well as theoretical[22−28] studies have been performed for various mutations in this region including the Flemish (A21G), Dutch (E22Q), Italian (E22K), Arctic (E22G), Iowa (D23N), and Osaka (ΔE22, deletion) variants. On the other hand, the regions 1−8 of $Aβ_{40}$ and 1−16 of $Aβ_{42}$ were believed to be disordered in the fibril state,[29−31] and the mutation in the N-terminal has attracted little attention of researchers. However, recent experiments[32−34] have suggested that residues at the N-terminal may be ordered and this terminal could carry some structural importance. The English (H6R),[35,36] Taiwanese (D7H),[37] and Tottori (D7N)[36,38,39] mutations can alter the fibril formation rate and the survival of cells without affecting Aβ production.[36] The mutation A2V was found to enhance Aβ40 aggregation kinetics, but the mixture of the Aβ40 wild type (WT) and A2V peptides protects against AD.[40] Using single-molecule AFM force spectroscopy, one can show that the N-terminal plays a key role in the peptide interaction in Aβ dimers.[41]

Received: January 23, 2014
Revised: June 19, 2014
Published: June 20, 2014

The all-atom replica exchange molecular dynamics (MD) simulations were performed to understand the influence of the mutation A2V on the equilibrium ensemble of the truncated peptide $A\beta_{1-28}$.[42] The impact of D7N on the aggregation and structure dynamics of alloforms $A\beta_{40}$ and $A\beta_{42}$ has been studied in our previous simulations.[43] In this paper, a similar study is conducted but for the English mutation H6R using all-atom MD simulations at 300 K in explicit solvent within the microsecond time scale. Our goal is to understand at the atomistic level the influence of this mutation on random coil monomeric structures and fibrillar-like dimeric structures of $A\beta_{40}$ and $A\beta_{42}$. By using simple reaction coordinates such as the β-strand content, global reaction coordinates, and principal component analysis to construct free energy landscapes and studying the dynamics of the salt bridge (SB) network, we can provide structural and physical insights into the experimental observation that the H6R mutation modulates the early steps of aggregation and enhances the rate of fibril formation.[39] Having estimated the solvation free energy, it was shown that the mutation increases the hydrophobicity of $A\beta$ peptides, accelerating their association. In addition, we predict that H6R has little impact on the collision cross section (CCS) of monomers as well as oligomers of $A\beta$ peptides.

RESULTS AND DISCUSSION

Equilibration Times. Figure S1 in the Supporting Information (SI) shows the time evolution of the potential energies of the WT and H6R $A\beta_{42}$ monomers and dimers. The time for the energy to equilibrate varies from 100 (monomer) to 200 (dimer) ns. The same equilibration times τ_{eq} have been obtained for $A\beta_{40}$ systems (results not shown). The fact that $\tau_{eq} \approx 100$ ns for monomers and 200 ns for dimers is also supported by the time dependence of secondary structures, the gyration radius R_g (Figures S2−S4 in the SI), and the hydrophobic and hydrophilic solvent accessible surface area (Figures S5 and S6 in the SI). Note that Figures S2−S6 show results obtained for representative systems, while similar results for other systems are not shown. As a result, for monomers, we used snapshots collected in the last 650 ns for estimating all thermodynamics quantities. For the dimers, we used the last 600 ns starting from the fibrillar-like states (Figure 1) and the 300 ns generated in six 50 ns MD simulations starting from the most populated states.

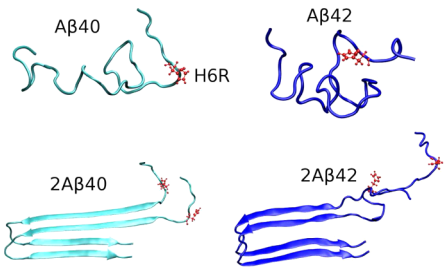

Figure 1. Initial structures for MD simulations of monomers and dimers with H6R sequences. The residue 6, where the mutation is made, is shown in red.

It should be stressed that the results obtained for all WT systems have been already reported in our previous work,[43] but we show them again to better clarify the effect of H6R mutation on structural dynamics and assembly dynamics.

Impact of H6R on the Secondary Structures, Salt Bridge Populations, and Collision Cross Sections of $A\beta_{40}$ and $A\beta_{42}$ Monomers. The mean and standard deviation of secondary structures of the four monomers are reported in Table 1. The mutation does not change much the secondary structure of $A\beta_{40}$. The coil and turn dominate and fluctuate around 40 and 53% in WT versus 37 and 57% in H6R with the same standard deviations. In both species, the β-strand and α-helix contents remain marginal, 6 and 3%, respectively. In contrast, the secondary structure of $A\beta_{42}$ changes upon H6R mutation. Within the error bars, the β-structure remains essentially the same but the helix content increases from 1 to 8%. While in WT, the coil dominates with 42%, followed by the turn (36%) and β-strand (21%); in H6R, the turn dominates with 52%, followed by the coil (24%) and the β-strand (16%). There is therefore an increase of 16% of turn and a decrease of 18% of coil upon H6R mutation. The similar effect on turn, coil and β-structure was obtained by the Tottori familial disease mutation (D7N).[43]

To obtain more details on the impact of H6R on $A\beta_{40}$ and $A\beta_{42}$ monomers, one considers the secondary structure propensity along the sequence (Figure 2). While the averaged contents over all residues are rather similar for both $A\beta_{40}$ species, the per-residue propensities differ for β-strand, α-helix, turn, and coil. $A\beta_{40}$-WT is rich in beta structure at residues Arg5 and Met35, while the propensity levels up at amino acids 4 and 38 upon mutation. This minor change does not allow one to draw any conclusion about the mutation effect on the self-assembly kinetics of $A\beta_{40}$. $A\beta_{42}$-WT is β-rich at Arg5, Lys6, Val18, Phe19, 26, Asn27, Lys28, 36, 37, 40 and 41, whereas $A\beta_{42}$-H6R is β-rich at Val18, 26, Lys28, 32, 33, 34, 35, 39, Val40, and Ile41. Since the region 1−16 is disordered in the fibrillar state, the reduction of β-content at Arg5 and Lys6 presumably supports the enhancement of propensity to aggregation. The decrease of β-content at Asn27 and Lys28 in the loop region and the noticeable increase of β-content at the C-terminal imply that, in accord with the experiment[36] and the general theoretical argument[44,45] about the role of the fibril-prone state, H6R speeds up the fibril growth of $A\beta_{42}$. The helix propensity remains very low along the sequence of both $A\beta_{40}$ species, while for $A\beta_{42}$ it levels up in the disordered region 14−16 upon mutation. The enhancement of helix content in the loop region 23−25 may make the loop more rigid facilitating the $A\beta_{42}$ aggregation. The increase of the turn content in the loop region 25−29 by about 30% also supports the acceleration of $A\beta_{40}$ self-assembly upon H6R mutation. In $A\beta_{42}$, the impact of substantial reduction of the turn at residues 23−26 is canceled out by its increase at 27−29 residues as they are from the same loop region, but the increase of the turn content in the C-terminal disfavors the fibril formation. The enhancement of the coil in the disordered region 1−8 of $A\beta_{40}$ and the reduction in regions 10−13, 26−29, and 30−34 would render conformations more favorable for aggregation. In $A\beta_{42}$, the substantial decrease of the coil, particularly in the C-terminal, clearly supports the experimental finding[36] that H6R facilitates the fibril growth of alloforms $A\beta$ peptides.

At neutral pH, both $A\beta_{42}$-WT and $A\beta_{40}$-WT species have six negatively charged residues (Asp1, Glu3, Asp7, Glu11, Glu22, and Asp23), and three positively charged residues (Arg5, Lys16 and Lys28). Therefore, one has $3 \times 6 = 18$ possible intramolecular SBs. The mutation H6R adds one positively charged residue 6R increasing the number of SBs to $4 \times 6 = 24$. We have studied lifetimes and population distributions of all SBs for WT and H6R sequences. Figure 3 shows the population of SB 22−28 and 23−28 for WT and H6R monomers. In $A\beta_{40}$, the mutation makes SB22−28 less rigid leaving the flexibility of SB 23−28 almost unchanged, but their populations remain low for both WT and H6R (Table 2). For $A\beta_{42}$, H6R mutation substantially

dx.doi.org/10.1021/cn500007j | ACS Chem. Neurosci. 2014, 5, 646−657

Table 1. Mean and Standard Deviation of Secondary Structure. Structures Were Obtained by Using the Last 650 ns for the Monomers, and the Last 600 ns from the Long Run and 300 ns from Six Short Runs Starting from Dominant Conformations for the $A\beta_{40}$ and $A\beta_{42}$ dimers with H6R Sequences[a]

	$A\beta_{40}$		$A\beta_{42}$		$2A\beta_{40}$		$2A\beta_{42}$	
content (%)	WT	H6R	WT	H6R	WT	H6R	WT	H6R
β	6 ± 2	3 ± 2	21 ± 1	16 ± 9	32 ± 3	15 ± 3	24 ± 2	27 ± 2
α	1 ± 2	3 ± 3	1 ± 1	8 ± 2	1 ± 1	0 ± 1	0 ± 1	5 ± 1
turn	53 ± 7	57 ± 8	36 ± 3	52 ± 12	29 ± 4	45 ± 6	49 ± 3	33 ± 3
coil	40 ± 7	37 ± 8	42 ± 3	24 ± 4	38 ± 6	40 ± 5	26 ± 4	35 ± 5

[a]Standard deviations are calculated using block analysis. The data of the WT systems were published in our previous work.[43]

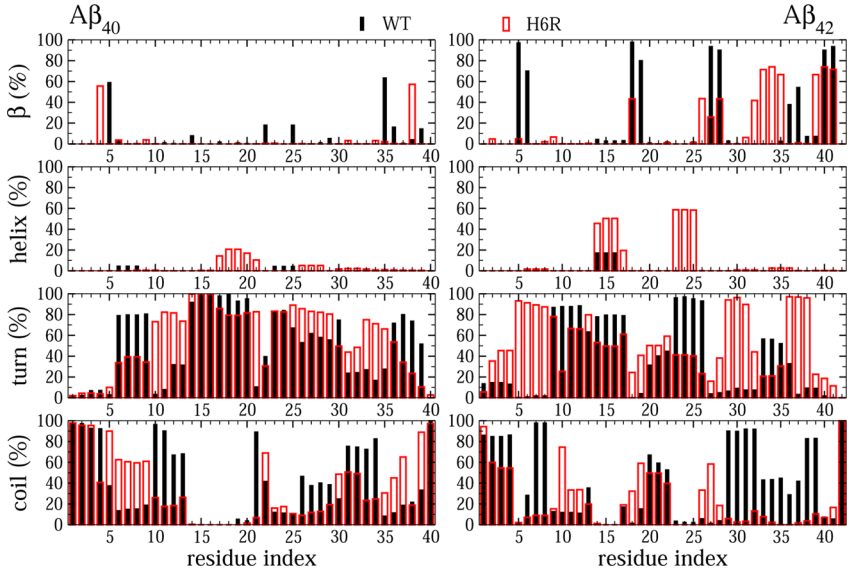

Figure 2. Probabilities of secondary structure in WT (black) and H6R (red) $A\beta_{40}$ and $A\beta_{42}$ monomers. Results are obtained from the last 650 ns of MD simulations (the first 100 ns was excluded).

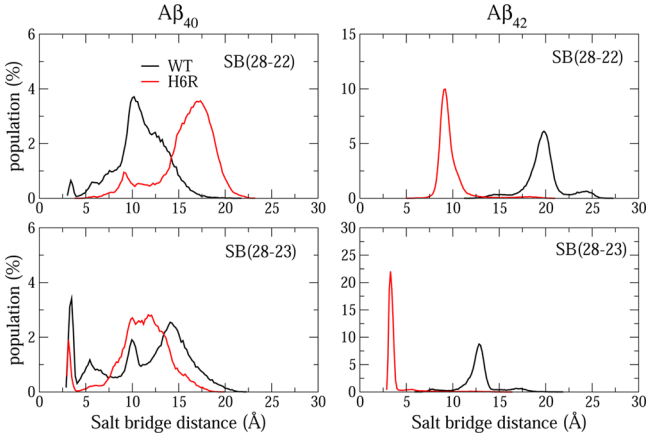

Figure 3. Population of intra 28−22 (upper panels) and 28−23 (lower panels) salt bridge distances in the monomers $A\beta_{40}$ and $A\beta_{42}$ with WT (black) and H6R (red) sequences.

reduces the distances of SB22−28 and SB23−28 and the population of the latter increases from 0 to 95% (Table 2). On the other hand, the recent experiment[46] showed that the aggregation rate of $A\beta_{40}$-lactam[D23-K28], in which the residues D23 and K28 are chemically constrained by a lactam bridge, is nearly a 1000 times greater than in the wild-type. This is because the SB constraint increases the population of the fibril-prone **N*** conformation in the monomer state[44] leading to faster aggregation.[45,47,48] From this point of view H6R would speed up the self-assembly as it makes the SB23−28 bridge more rigid.

Table 2 also shows the mutation effect on the propensity of SBs 1−6, 3−6, 6−11, 6−22, and 6−23. In $A\beta_{40}$, the substantial increase is obtained for 6−22 (42%), while in $A\beta_{42}$ the lifetime levels up by 66, and 54% at SB 1−6, and 3−6, respectively.

Experimental cross sections measured for each dehydrated monomer are 679 ± 8 Å^2 for $A\beta_{40}$ and 693 ± 8 Å^2 for $A\beta_{42}$,[49] and the Tottori (D7N), Flemish (A21G), and Arctic (E22G), known as familial AD, mutants have no noticeable effect on $A\beta$ monomer cross section. Using dehydrating and energy-minimizing dominant structures and the trajectory method,[50] we have obtained[43] the mean value of CCS of 760, 765, 740, and 757 Å^2 for $A\beta_{40}$-WT, $A\beta_{42}$-WT, $A\beta_{40}$-D7N, and $A\beta_{42}$-D7N, respectively. Within error bars of 4%, these results fall to the same range of experimentally observed CCS. Note that Baumketner et al. also determined a CCS of 765 Å^2 for $A\beta_{42}$-WT using replica exchange MD with a generalized Born approximation.[51]

CCS of monomers with H6R mutation has not been studied experimentally. Here we estimate CCS using dominant structures characterizing local basins on the free energy surface (FES) obtained by the dihedral principal component analysis for each system. The FES of $A\beta_{40}$-H6R and $A\beta_{42}$-H6R are characterized by 4 and 5 free energy minima (Figure S7), with CCS values of 734, 743, 747, and 721, and 732, 767, 705, and 770 Å^2, respectively. The error bars for the calculated CCS is about 3.5%. Thus, together with D7N, A21G and E22G, H6R has a minor influence on CCS of $A\beta$ monomers.

dx.doi.org/10.1021/cn500007j | ACS Chem. Neurosci. 2014, 5, 646−657

Table 2. Population (%) of Intramolecular Salt-Bridges Formed in the Monomer and Dimer Systems[a]

	1−6	3−6	11−6	22−6	23−6	22−28	23−28
$A\beta_{40}$-WT	0 ± 0	0 ± 0	0 ± 0	0 ± 2	0 ± 2	2 ± 1	12 ± 3
$A\beta_{40}$-H6R	9 ± 2	12 ± 2	0 ± 0	42 ± 4	0 ± 0	0 ± 0	5 ± 2
$A\beta_{42}$-WT	0 ± 0	0 ± 0	0 ± 0	0 ± 0	0 ± 0	0 ± 0	0 ± 0
$A\beta_{42}$-H6R	66 ± 5	54 ± 4	10 ± 2	0 ± 0	0 ± 0	0 ± 2	90 ± 5
$2A\beta_{40}$-WT	0 ± 0	0 ± 0	0 ± 0	0 ± 0	0 ± 0	41 ± 3	18 ± 4
$2A\beta_{40}$-H6R	6 ± 2	3 ± 1	52 ± 4	0 ± 0	0 ± 0	5 ± 1	19 ± 3
$2A\beta_{42}$-WT	0 ± 0	0 ± 0	0 ± 0	0 ± 0	0 ± 0	3 ± 1	53 ± 4
$2A\beta_{42}$-H6R	25 ± 4	2 ± 1	41 ± 5	0 ± 0	0 ± 0	34 ± 3	15 ± 2

[a]The salt bridge distances are calculated between the atom CG (in ASP1 or ASP23) or CD (in GLU3, GLU11 or GLU22) and the atom NZ (in LYS28) or NH2 (in ARG6) or NE2 (in HIS6). The cutoff distance used for considering one SB formed is 0.46 nm. The data use the last 650 ns for the monomers, and the last 600 ns from the long run and 300 ns from six short runs starting from dominant conformations for the $A\beta_{40}$ and $A\beta_{42}$ dimers with H6R sequences.

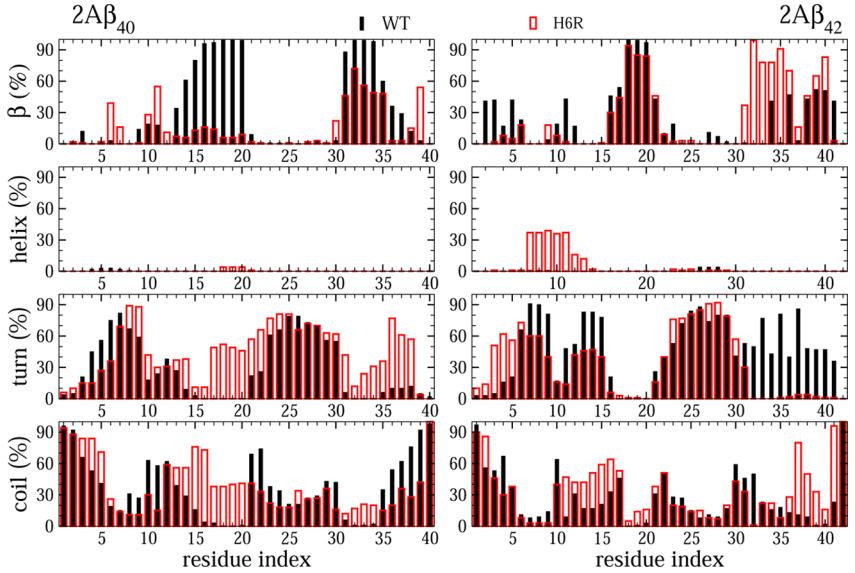

Figure 4. Distributions of secondary structure in WT (black) and H6R (red) $A\beta_{40}$ and $A\beta_{42}$ dimers. Results were obtained from the last 600 ns (the first 200 ns was excluded) from the long run and 300 ns from six short runs starting from dominant conformations for the $A\beta_{40}$ and $A\beta_{42}$ dimers with H6R sequences. The data sampling WT systems was described previously.[43]

Mutation Enhances Hydrophobicity of $A\beta_{40}$ and $A\beta_{42}$ Monomers. To study the effect of H6R on hydrophobicity of monomers, we calculate the solvation free energy $G_{solvation}$ using the molecular mechanics Poisson−Boltzmann surface area (MM-PBSA) method[52] (more details may be found in our previous works[53,54]) where $G_{solvation}$ was approximated as the sum of electrostatic and nonpolar contributions, $G_{solvation} = G_{PB} + G_{sur}$. Here G_{PB} derived from the electrostatic potential between solute and solvent was determined using the continuum solvent approximation.[55] Using grid spacing 0.1 Å, the APBS package[56] was implemented for numerical solution of the corresponding linear Poisson−Boltzmann equation. The GROMOS radii and charges were used to generate PQR files. Then, the nonpolar solvation term G_{sur} was approximated as linearly dependent on the solvent accessible surface area (SASA), derived from Shrake-Rupley numerical method[57] integrated in the APBS package. $G_{sur} = \gamma SASA + \beta$, where $\gamma = 0.0072$ kcal/mol·Å ^{2} and $\beta = 0$.[58]

Because the mutation changes the net charge, it has much stronger impact on the electrostatic contribution G_{PB} than the nonpolar term G_{sur} (Table S2 in the SI). Upon mutation, the solvation free energy of $A\beta_{40}$ levels up from −594.2 to −501.7 kcal/mol. A more pronounced increase was observed for $A\beta_{42}$. Thus, by reduction of the net charge, mutation H6R makes both monomers more hydrophobic, enhancing their propensity to fibril formation as observed in experiments.

Impact of H6R on the Secondary Structure, Salt Bridge Formation, and CCS in $A\beta_{40}$ and $A\beta_{42}$ Dimers. The overall β-strand content of $2A\beta_{42}$ remains essentially the same upon mutation (Table 1), but we see variations along the sequence (Figure 4). The visible decrease occurs in the disordered region 2−12, while it slightly drops at residues 16−21. The enhancement of β-structure at the C-terminal is in accord with the experimental finding that the English mutation accelerates aggregation of alloforms $A\beta$ peptides. A moderate change in α-helix at residues 7−11 presumably does not affect much the kinetics of fibril growth. The turn drops from 49% in $2A\beta_{42}$-WT to 33% in $2A\beta_{42}$-H6R but leaving the CHC and loop region untouched (Figure 4). The substantial decrease of the turn in the C-terminal also supports the promotion of aggregation by H6R. The mutation levels up the coil from 26% in WT to 35% in H6R and mainly impacts regions 11−16 and 36−41. The increase of coil in the C-terminal may suggest that the mutation retards aggregation, but this effect is probably compensated by the huge decrease of the turn in the same region. Taken together, our simulations support the enhancement of aggregation of $A\beta_{42}$ by the English mutant.

dx.doi.org/10.1021/cn500007j | ACS Chem. Neurosci. 2014, 5, 646−657

Upon mutation, the β-structure decreases from 32% in 2Aβ_{40}-WT to 15% in 2Aβ_{40}-H6R (Table 1). The reduction takes place at residues 13−20 and 31−35, whereas the visible enhancement occurs at residues 6, 10, and 39 (Figure 4). There is almost no helix in both species. The percentage of turn in 2Aβ_{40}-WT (29%) is lower than 2Aβ_{40}-H6R (45%). The mutation significantly impacts the CHC region and residues 15, 16, 31, and 35−38. The mean percentage of coil is nearly the same for WT (38%) and H6R (40%), but we observe variations along the amino acid sequences (Figure 4). The increase of coil occurs at residues 3−5 and 14−20 at the expense of its decrease at residues 10, 11, 22, 23, and 35−40. Overall, contrary to the 2Aβ_{42}, the mutation seems to disfavor aggregation as it makes 2Aβ_{40} less structured. This may be because the acquisition of fibril state of Aβ_{40} occurs at much longer time scales than Aβ_{42} and at the same simulation time scales 2Aβ_{40} species remain less ordered than 2Aβ_{42}. The support for enhancement of Aβ_{40} aggregation may be obtained from the intrapeptide SB dynamics, as upon mutation the lifetimes of SB 23−28 increases (Figure 5). The mutation effect is

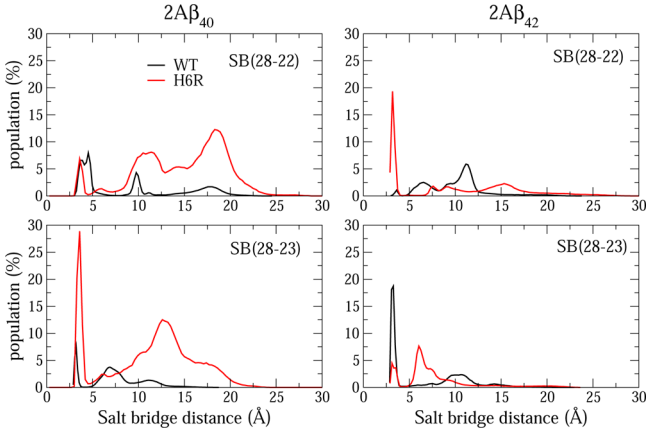

Figure 5. Population of intra 28−22 (upper panels) and 28−23 (lower panels) salt bridge distances in WT (black) and H6R (red) sequences of Aβ_{40} and Aβ_{42} dimers. Results were obtained from 600 ns (the first 200 ns was excluded) from the long run and additional 300 ns of short runs for dimer Aβ_{40} and Aβ_{42} systems.

less pronounced in Aβ_{42}, where the SB 22−28 becomes more rigid, but SB23−28 remains flexible. In 2Aβ_{40}-WT, the most populated are SBs 22−28 (41%) and 23−28 (18%) (Table 2), while in 2Aβ_{40}-H6R they are 6−11 (52%) and 23−28 (19%). For 2Aβ_{42}-WT, only the SB 23−28 has the high lifetime (53%), while H6R has the population of SBs 1−6, 6−11, and 22−28 exceeding 25%.

Figure S8 in the SI shows the populations of interpeptide SB 22−28 and 23−28 for all dimer species. In 2Aβ_{40}-WT, SB 22−28 has very short lifetime of 3% (Table S2 in the SI), while upon mutation these SBs are not populated through the whole MD run. The noticeable increase of the lifetime of SB23−28 from 6% to 45% by mutation suggests that, in agreement with the experiments, H6R accelerates fibril growth of Aβ_{42}. The mutation levels up the population of SB 6−11 of 2Aβ_{40} (from 0 to 65%) and 1−6 for 2Aβ_{42} (from 0 to 38%).

Impact of H6R on the Free Energy Surfaces of Aβ_{40} and Aβ_{42} Dimer. Using PCA and snapshots collected in the full trajectory of 800 ns and six trajectories of 50 ns, the FES of 2Aβ_{40}-WT and 2Aβ_{40}-H6R have been constructed (Figure 6) to understand the impact of mutation on the fibrillar-like states. The FES of 2Aβ_{40}-H6R with seven free energy basins is broader and more

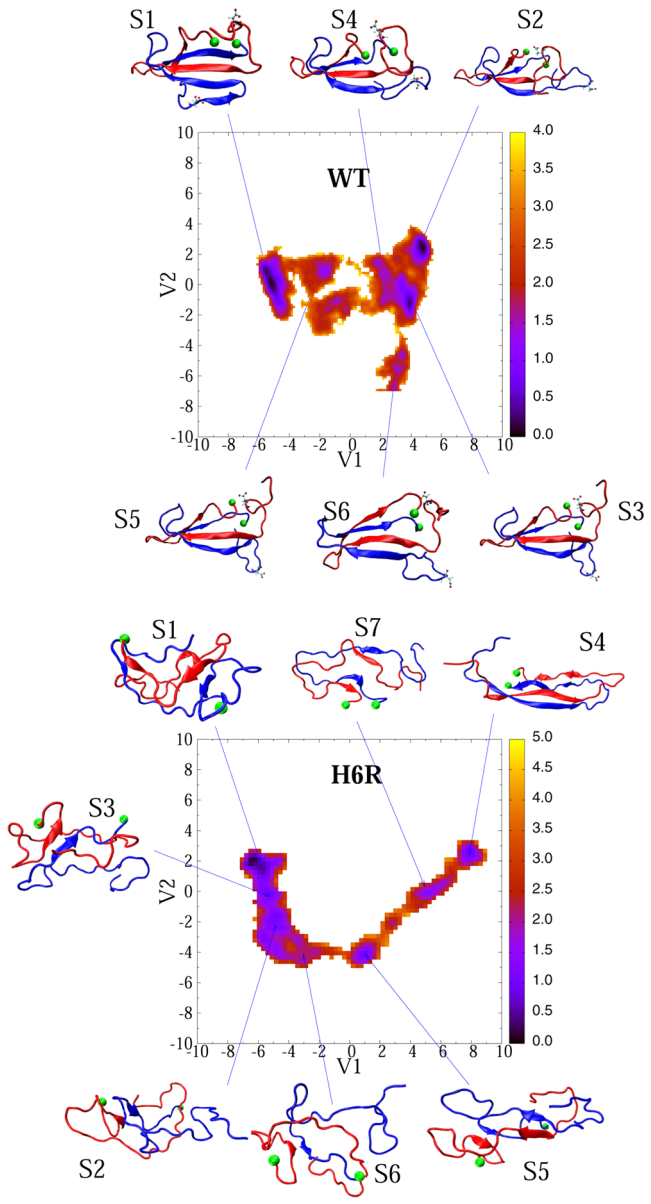

Figure 6. Free energy landscape of 2Aβ_{40}-WT (upper) and 2Aβ_{40}-H6R (lower) as a function of the first two principal components V1 and V2 obtained from the PCA analysis on the inverse of inter side-chain distances. The conformations corresponding to each free energy minima are shown. The C-terminus amino acid of all structures is shown by a green ball. Units are in kcal/mol.

complex than WT that has six local minima. Our previous study[43] yields a similar result for the Tottori mutation D7N which also makes the FES of Aβ_{40} dimer more complicated. Table 3 gives for each free energy local minima its population, the mean value of fibril contacts (N_{fb}), the distance between centers of mass of residues 6 from two chains, the secondary structure composition, the n-stranded β-sheet topology, and the CCS.

Upon mutation, the charge of N-terminal is reduced, resulting in a weaker repulsion between two chains. As a result, the two N-termini are far apart in the WT dimer (the mean distance between two residues 6 is 21 Å), while they are close in promixity in H6R with the mean distance between two residues 6 of 7 Å (Table 3).

In terms of the secondary structure composition, six dominant structures of WT are remarkably similar (Figure S9 in SI) but

dx.doi.org/10.1021/cn500007j | ACS Chem. Neurosci. 2014, 5, 646−657

Table 3. Characterization of the Conformational States (S) of the WT and H6R Aβ40 Dimers Indicated on the Free Energy Landscapes Shown in Figure 6[a]

system	S	P	N_{fb}	d_{R6}	β	α	turn	coil	iP_{bs}^{2s}	oP_{bs}^{2s}	P_{bs}^{3s}	P_{bs}^{4s}	CCS
2Aβ_{40}-WT	1	36	16	2.21	33	1	30	36	29	0	4	67	1279
	2	19	14	1.78	32	0	33	35	2	19	4	89	1347
	3	18	16	2.39	34	0	27	38	0	26	0	96	1211
	4	9	15	2.51	30	0	26	44	0	0	0	100	1297
	5	7	16	2.59	29	0	22	48	0	0	0	100	1387
	6	6	19	1.82	34	0	25	41	0	0	0	100	1275
2Aβ_{40}-H6R	1	39	7	0.60	15	1	46	38	0	59	0	0	1281
	2	19	7	111	9	0	48	43	0	13	0	0	1289
	3	12	8	0.76	14	0	47	39	2	57	0	0	1311
	4	8	29	0.58	40	0	17	43	0	100	26	17	1548
	5	8	9	0.47	16	0	37	48	0	44	0	0	1290
	6	8	8	1.03	12	0	45	43	0	0	0	0	1363
	7	6	15	0.55	16	0	25	59	0	79	0	0	1380

[a]Shown are the population P (in %), the mean values of the total fibril contacts (N_{fb}), the center of mass distance between the 6th residues of two chains (d_{R6}), the secondary structure contents (in %) using residues 1−40, the populations (in %) of intramolecular 2-stranded β-sheet (iP_{bs}^{2s}), intermolecular 2-stranded β-sheet (oP_{bs}^{2s}) 3-stranded β-sheet (P_{bs}^{3s}) and 4-stranded β-sheet (P_{bs}^{4s}). The populations of higher-stranded β-sheets are almost zero. The CCS (in Å^2) are given.

their *n*-stranded β-sheet topologies are different. The lifetime of the intramolecular 2-stranded β-sheet of structure S1 is relatively high (29%), while the intermolecular 2-stranded β-sheet topology is rich for S2 and S3 with a minor population of P_{bs}^{3s} for all basins. The seven representative structures of 2Aβ_{40}-H6R are more extended and less compact than the six WT structures with formation of short β-strands at the C-terminus (Figure 6). The secondary structures, especially the β-composition greatly vary from minima to minima (Table 3 and Figure S9). The basin S4 has the highest β-content (40%), but the turn (17%) is lowest. The mutation has the pronounced influence on the intermolecular 2-stranded β-sheet topology with the mean value of oP_{bs}^{2s} averages 8 and 49% for WT and H6R, respectively. This result supports the experimental observation on the acceleration of aggregation by mutation. The minor effect of mutation is seen for the interchain 3-stranded β-sheets as one has 4% for basins S1 and S2 but relatively high (26%) for structure S4 (Table 3). Upon mutation, the population the 4-stranded β-sheet is substantially reduced signalizing about the loss of long-range ordering.

Using ion-mobility mass spectrometry, Bernstein et al.[49] reported a CCS of 1142 Å^2 for the dimer of Aβ_{40}-WT with an accuracy of ±1%, but CCS of 2Aβ_{40}-H6R has not been determined. The six representative structures (Figure 6) have slightly higher CCS values than the experimental ones (see Table 3 and the discussion in our previous paper[43]). CCS of seven local minima structures of two Aβ_{40}-H6R are higher than the experimentally determined value for WT, and their mean value is 1351 ± 88 Å^2. The structure S4 with the highest value of CCS is richest in the β-structure. Upon the Tottori familial disease mutation D7N, a CCS of dimer Aβ_{40} is 1200 Å^2[49] which is a bit higher than the WT value. Since both H6R and D7N reduce the net charge of Aβ peptide, they are expected to have a similar impact on CCS. This is in line with our simulation results that CCS increases upon both mutations.

Figure 7 shows the FES of dimers Aβ_{42} with dominant structures obtained by the full trajectory of 800 ns and six additional trajectories of 50 ns starting from local basin conformations. The FES of H6R is compatible with WT in complexity having five main local minima for H6R against six minima for WT. The structural characteristics of each local free energy structure are presented in Table 4. The β-structure propensity varies along the sequence of H6R to less extent than WT (Figure S10 in the SI), suggesting that the system becomes more stable upon mutation.

The first two minima, representing 59% and 72% of all conformations for the WT and H6R sequences, have the mean number of fibril contacts 9 and 17 in WT and H6R sequences versus 40 in the NMR fibril state. Contrary to the dimer Aβ_{40} (Figure 6), the two C-termini of all dominant structures of 2Aβ_{42}-H6R are very close in promixity (Figure 7), implying that upon mutation dimer Aβ_{42} becomes a good catalyst for seeding growth of fibril. This is also consistent with higher β-structures and percentages of intermolecular 2- and 3-stranded β-sheets (Table 4) of H6R versus WT. The populations of the intermolecular 4-stranded sheets of dominant structures of WT are, however, higher than those of the mutant. Upon reduction of the net charge, the distance between residues 6 of Aβ_{42} dimer is reduced but to less extent compared to the Aβ_{40} case (compare Tables 3 and 4).

According to Bernstein et al.,[49] CCS of 2Aβ_{42}-WT is 1256 Å^2 with an accuracy of ±1%. Our theoretical estimation of CCS using six dominant structures in Figure 7 give a satisfactory agreement with the experiment (Table 3 and ref 43). Although CCS of mutant 2Aβ_{42}-H6R has not been determined, we computed it using five dominant structures (Figure 7) and the trajectory method.[50] As follows from Table 4, their mean value of 1432 ± 74 Å^2 is higher than the experimental estimate for WT, and within the error bars it falls into the range of 2Aβ_{40}-H6R. Therefore, similar to Aβ_{40}, mutation H6R seems to increase CCS of dimer Aβ_{42}. Having used the same theoretical approach,[50] we have obtained CCS of 1319 ± 69 Å^2 for 2Aβ_{40}-D7N[43] which is also in the range of 2Aβ_{40}-H6R. Thus, in accord with the experiments of Bernstein et al.,[49] CCS of Aβ dimers is not sensitive to mutations.

COMPARISON BETWEEN H6R AND D7N

Our results on secondary structures of WT monomers and dimers have been already compared with the results of other groups in detail.[43] Here we rather focus on differences between English and Tottori mutations in terms of their impact on structural changes and assembly of Aβ_{40} and Aβ_{42}.

dx.doi.org/10.1021/cn500007j | ACS Chem. Neurosci. 2014, 5, 646−657

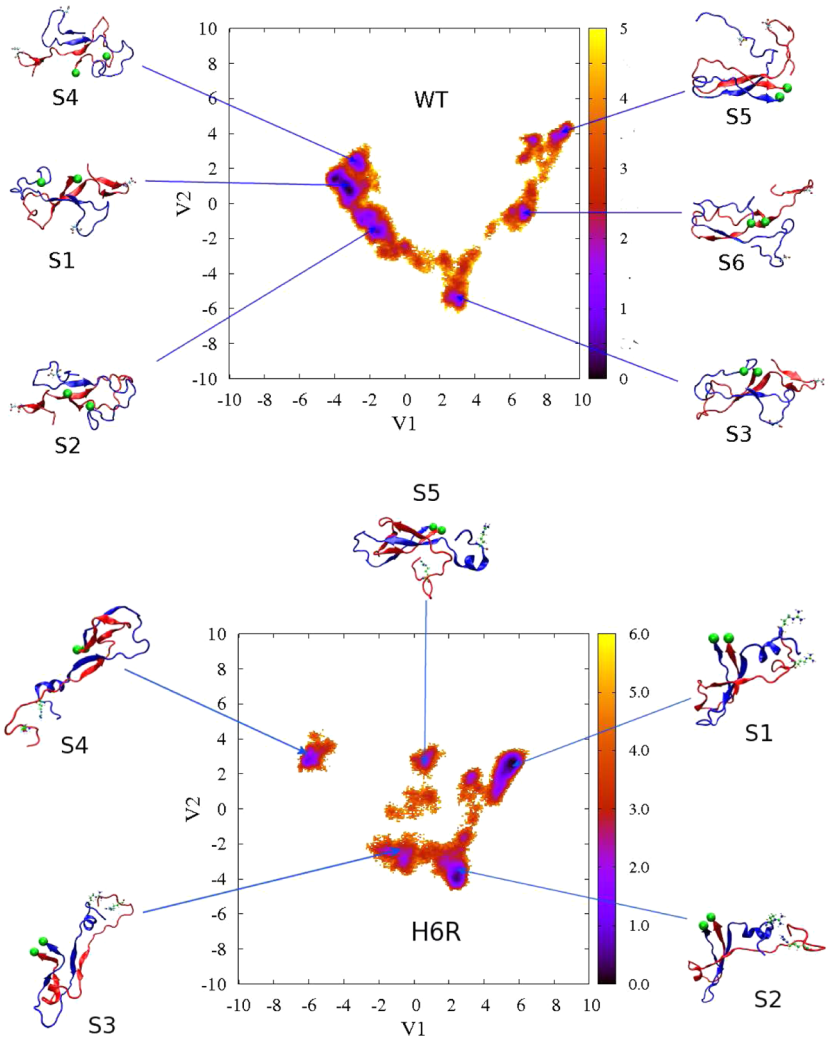

Figure 7. Free energy landscape of 2Aβ_{42}-WT (upper) and 2Aβ_{42}-H6R (lower) as a function of the first two principal components V1 and V2 obtained from the PCA analysis on the inverse of inter-side-chain distances. The conformations corresponding to each free energy minima are shown. Residues 6th are shown explicitly. The C-terminus amino acid of all structures is shown by a green ball. Units are in kcal/mol.

Table 4. Characterization of the Conformational States (S) of the Aβ42-WT Dimer Aβ42-H6R Dimer Indicated on the Free Energy Landscapes Shown in Figure 7[a]

system	S	P	N_{fb}	d_{R6} (nm)	β	α	turn	coil	iP^{2s}_{bs}	oP^{2s}_{bs}	P^{3s}_{bs}	P^{4s}_{bs}	CCS
2Aβ_{42}-WT	1	35	8	1.8	23	0	51	26	22	0	14	85	1342
	2	24	9	1.6	24	1	47	28	27	0	12	87	1292
	3	9	12	1.9	26	0	43	31	23	0	9	90	1339
	4	8	8	2.2	25	0	51	24	20	2	10	88	1351
	5	7	24	3.1	27	0	23	50	0	99	0	0	1566
	6	6	18	2.9	25	0	37	38	24	2	76	20	1441
2Aβ_{42}-H6R	1	42	17	1.4	28	6	29	36	7	75	65	42	1357
	2	30	17	0.9	27	4	34	33	2	60	41	47	1428
	3	11	16	1.2	20	6	42	29	1	81	36	2	1532
	4	10	16	0.9	21	6	49	23	6	97	0	0	1497
	5	5	18	2.0	32	1	39	26	10	27	43	38	1346

[a]Shown are the population P (in %), the mean values of the total fibril contacts (N_{fb}), the center of mass distance (in nm) between the 6th residues of two chains (d_{R6}), the secondary structure contents (in %) using residues 1−42, the populations (in %) of intramolecular 2-stranded β-sheet (iP^{2s}_{bs}), intermolecular 2-stranded β-sheet (oP^{2s}_{bs}), 3-stranded β-sheet (P^{3s}_{bs}), and 4-stranded β-sheet (P^{4s}_{bs}). The populations of higher-stranded β-sheets are almost zero.

The effect of D7N and H6R on the monomer folding of Aβ peptides has not been experimentally studied, but some information may be inferred from the present theoretical study. Our monomer simulations show that the secondary structures of Aβ_{42} change to greater extent than Aβ_{40} upon both mutations (Table 1 and ref 43). Thus, the mutation effect on the folding rate and conformational dynamics should be more pronounced for Aβ_{42} than for Aβ_{40}. For each peptide, the mutation effects are expected

dx.doi.org/10.1021/cn500007j | ACS Chem. Neurosci. 2014, 5, 646−657

to be different because the per-residue distributions of secondary structures are different for D7N[43] and H6R (Figure 2).

A turn at Ser8-Gly9 might be particularly important because it can bring the N-terminal quarter of the peptide into contact with the CHC region, modulating substantially the Aβ assembly kinetics.[59] Being in proximity with the putative Ser8-Gly9 turn, the mutations H6R and D7N may affect it and through this effect alter the aggregation rate.[39] This point of view is supported by simulations on all D7N species with an increased turn propensity at residues 5−12 (Aβ_{40} monomer) and 1−9 (Aβ_{42} monomer), as well as a decreased turn propensity at residues 6−9 in both dimers.[43] Upon H6R mutation the turn content at Ser8-Gly9 decreases in Aβ_{40} monomer and Aβ_{42} dimer but it increases in Aβ_{42} monomer and Aβ_{40} dimer (Figures 2 and 4). Thus, the impact of two mutations is similar for Aβ_{42} species but different for Aβ_{40} ones.

The experimental study of temporal changes in the secondary structure[39] revealed that both mutations H6R and D7N accelerate the conversion from random coil to β-sheet via α-helix by ≈10-fold in Aβ_{40} and ≈5-fold in Aβ_{42} system.[39] This is in qualitative agreement with our monomer simulations providing 3 and 18% reduction of coil in Aβ_{40} and Aβ_{42} upon mutation H6R. The similar reduction of coil by 5 and 14% in Aβ_{40} and Aβ_{42}, respectively, upon mutation D7N was obtained in our previous paper.[43] In contrast, our dimer simulations show that the coil content remains constant in Aβ_{40} upon both mutations, but increases by 9% by H6R and 16% in Aβ_{42} by D7N.[43] Since CD measures averaging structures, and monomers and dimers coexist in equilibrium with oligomers of higher orders, it is possible that dimeric structures exist with a richer coil-composition. The enhancement of aggregation rates obtained by the change in the bending free energy of SB 23−28 yields the maximum increase of ≈6-fold by H6R and ≈11-fold by D7N.[43] Given the crude approximation, we use these estimations that are in reasonable agreement with the experiment.

Experimental examination of the stabilized oligomers showed that H6R is more ordered than D7N.[39] This is consistent with our dimer simulations on Aβ_{42}, giving the β-content of 11% for D7N[43] versus 27% for H6R (Table 1). However, the results obtained for Aβ_{40} do not support this rank order as we have 36% and 15% β-structure for D7N and H6R, respectively. One of possible reasons is that the system contains oligomers of different orders and the rank ordering reported by Ono et al.[39] is controlled not only by dimers but also by other oligomers.

Robustness of Results against Force Fields. To check the robustness of our results against the choice of force field, we have performed additional simulations for dimer systems using the AMBER force field 99SB[60] and water model TIP3P[61] which is the best choice for this force field.[62,63] For each system, five 100 ns MD runs were carried out starting from dominant structures characterizing main basins on the FES. For comparison, a similar set of simulations was performed with the OPLS/AA force field and water model TIP4P. Figures S11 and S12 in the SI show the time dependencies of the gyration radius obtained by two force fields. Clearly, the systems are in equilibrium for the whole run of 100 ns as R_g fluctuates around its equilibrium value (similar results were obtained for secondary structures, the interaction energy and SASA (results not shown)). Snapshots collected every 10 ps during 100 ns were used to estimate equilibrium quantities. As evident from Table 5, the gyration radius, distance between centers of mass of residues 6 from two chains d_{R6-R6}, and β- and α-contents are not sensitive to force fields. A visible difference in turn and coil was observed for 2Aβ_{40}-H6R, where the turn is 40% in OPLS against 34% in AMBER but the coil content in OPLS (41%) is lower that than in AMBER (51%). Since the sum of the coil and turn is near the same in two force fields, the choice of force field would not impact the behavior of 2β_{40}-H6R.

Table 5. Comparison between Results Obtained by OPLS/AA and AMBER 99SB Force Fields for Dimers 2Aβ_{40}-WT, 2Aβ_{42}-WT, 2Aβ_{40}-H6R, and 2Aβ_{42}-H6R[a]

system	R_g (nm)	d_{R6-R6} (nm)	β	α	turn	coil
2Aβ_{40}-WT-OPLS	1.55	1.73	32	0	29	39
2Aβ_{40}-WT-AMBER	1.52	1.77	33	0	27	40
2Aβ_{42}-WT-OPLS	1.44	2.10	23	0	46	31
2Aβ_{42}-WT-AMBER	1.51	1.96	21	2	41	36
2Aβ_{40}-H6R-OPLS	1.50	1.35	18	1	40	41
2Aβ_{40}-H6R-AMBER	1.49	1.31	14	1	34	51
2Aβ_{42}-H6R-OPLS	1.68	1.42	27	5	32	36
2Aβ_{42}-H6R-AMBER	1.69	1.39	25	4	30	41

[a]Shown are the gyration radius R_g, the distance between centers of mass of residues 6 of two chains d_{R6}, and secondary structure contents. The secondary structure contents are measured in %. Data were obtained from five extra 100 ns MD runs for each system.

Per-residue distributions of secondary structures obtained by OPLS and AMBER for four dimer systems are shown in Figures S13 and S14 in the SI. Because of their similarity, our results are expected to be independent of force field.

CONCLUSION

We have studied the influence of the H6R mutation on structure changes of Aβ monomers and dimers using long all-atom MD simulations in explicit water and a number of different methods for data analysis. Though sampling in the microsecond time scale might not be sufficient to converge to equilibrium, we are in a position to understand some experimental results at least at the qualitative level.

Upon mutation, the solvation free energy increases by an amount of about 92 and 194 kcal/mol for Aβ_{40} and Aβ_{42}, respectively. This pronounced effect clearly supports the acceleration of peptide self-assembly by increased hydrophobicity. Our data support the experimental finding that H6R speeds up fibril growth but the mechanisms are different for Aβ_{40} and Aβ_{42}. For both systems, we did not find an increase in overall β-strand content upon mutation. Rather we found that the enhanced aggregation rate of Aβ_{42} comes essentially from the local increase of β-content at the C-terminus for both monomeric and dimeric systems (β-structure of residues 30−42 levels up from 22% to 36% for monomer and from 22% to 51% for dimer), and from the mutation-induced rigidity of SB 23−28 of monomer. Without mutation, this SB is not formed during MD simulations, but in the presence of mutation its population becomes 90% (Table 2). In contrast, the enhanced aggregation rate of Aβ_{40} is associated with the increase of turn by 30% at residues 26−29 in the turn region and coil reduction at positions 10−13, 26−29, and 30−34 of the monomer as well as with decreased intramolecular SB 23−28 distance in the dimer.

We have shown that the English familial disease mutation has little impact on the CCS of alloform Aβ peptides, implying that this parameter is not sensitive enough to probe structural changes. Although CCS of H6R was not experimentally measured, our result is in qualitative agreement with the experiments, showing that other mutations like D7N, A21G, and E22G have no noticeable effect on CCS of both monomers and oligomers.

dx.doi.org/10.1021/cn500007j | ACS Chem. Neurosci. 2014, 5, 646−657

Although the simulations started from dimer conformations with the disordered N-terminal, our results are expected to be valid for the fibril model derived from patient brains[34] where the N-terminal is ordered, because the reduction of net charge upon H6R mutation always facilitates the fibril formation process independent of the nature of fibril structure.

Finally, for the first time, our study provides a detailed atomistic picture of conformational changes of $A\beta_{40/42}$ monomers and dimers upon the English mutation. Our results might be used to understand experimental findings on assembly kinetics and the collision cross section.

METHODS

Structures of the H6R $A\beta_{40}$ and $A\beta_{42}$ Monomers and Dimers. To generate the initial structures for sequences with mutation H6R, we used the same procedure as in our previous work.[43] We used NMR structures of full-length $A\beta_{40}$ (PDB code: 1BA4[64]) and $A\beta_{42}$ (PDB code: 1Z0Q[65]), resolved in a water-micelle solution, as starting configurations, and the OPLS force field[66] with TIP4P water model,[67] which is the most suitable for this force field.[62,63] We performed 5 ns MD simulations at 500 K to generate random coil conformations for WT monomers in aqueous solution.

The starting structures of the WT $A\beta_{40}$ and $A\beta_{42}$ dimers were taken from the NMR structures of $A\beta_{9-40}$ (PDB ID: 2LMN[29]) and $A\beta_{17-42}$ (PDB ID: 2BEG[31]), with addition of residues 1−8 from the heated $A\beta_{40}$ monomer and addition of residues 1−16 from the heated $A\beta_{42}$ monomer.

The initial structure of the H6R mutation was obtained from the WT final structure by using the mutation tools in PyMOL[68] for both monomer and dimer. The starting configurations for all MD simulations are shown in Figure 1. It should be noted that these configurations are the same as WT configurations in our previous work[43] except the residue H at position 6 is replaced by R.

Terminology. The $A\beta$ peptide was segmented into four regions: the N-terminal (residues 1−16), the central hydrophobic core (CHC) (residues 17−21), the fibril-loop region (residues 22−29), and the C-terminal (residues 30−42). For simplicity in what follows, the WT and H6R monomer and dimer will be referred to as $A\beta$40-WT, $A\beta_{40}$-H6R, $2A\beta_{40}$-WT, and $2A\beta_{42}$-H6R.

MD Simulations. The GROMACS 4.5.5 package[69] was used with the TIP4P water model[67] and the OPLS force field.[66] The OPLS-AA force field was used because the OPLS-generated conformations for the $A\beta_{40}$ and $A\beta_{42}$ monomer match reasonably the NMR data.[70] In addition, many studies have shown that OPLS is suitable for exploring the aggregation of several $A\beta$ fragments in explicit water[71] and gives results qualitatively similar to that found using the CHARMM force field for the $A\beta_{10-35i}$ dimer.[44] The equations of motion were integrated using a leapfrog algorithm[72] with a time step of 2 fs. The LINCS algorithm[73] was used to constrain the lengths of all covalent bonds with a relative geometrical tolerance of 10^{-4}. Temperature was controlled by the Bussi-Donadio-Parrinello velocity rescaling thermostat with a relaxation time of 0.1 ps found to sample the canonical ensemble.[74] The Berendsen pressure coupling method[75] was applied at a pressure of 1 atm. The van der Waals (vdW) forces were calculated with a cutoff of 1.4 nm, and the particle mesh Ewald method[76] was employed to treat the long-range electrostatic interactions. The nonbonded interaction pair list, with a cutoff of 1 nm, was updated every 10 fs.

In the simulations of $A\beta_{40/42}$ monomers, the species were centered in octahedron boxes of 57 Å with periodic boundary conditions containing about 4400 water molecules. For dimers, we used cubic boxes (the box size is 95 Å for $A\beta_{40}$ dimer and 92 Å for $A\beta_{42}$ dimers) with periodic boundary conditions that contain around 29 000 and 27 000 water molecules for the $A\beta_{40}$ dimers and the $A\beta_{42}$ dimers, respectively. Note that box sizes were chosen large enough to avoid artifacts that may be caused by periodic boundary conditions. Counterions Na^+ were added to neutralize each system. Each monomer was studied by 750 ns MD, and each dimer by 800 ns MD at 300 K. Additionally, we have performed six short runs of 50 ns for $2A\beta_{40}$-H6R and $2A\beta_{42}$-H6R, starting from dominant structures on the free energy surface, obtained from the long 800 ns run.

Analysis. *Contacts.* The time dependence on the number of hydrogen bonds (HB), side chain contacts, and salt bridges was monitored.[54] One HB was formed if the distance between donor D and acceptor A is ≤3.5 Å and the D−H−A angle is ≥135°. A SC−SC contact was considered as formed if the distance between their centers of mass is ≤6.5 Å. This condition was used to define the number of native contacts in $A\beta_{40}$ and $A\beta_{42}$ fibrils using the residues 9−40 in $A\beta$40 and 17−42 in $A\beta$42, leading to 51 and 40 fibrillar-like contacts, respectively. A native contact between residue i of peptide 1 and residue j of peptide 2 was formed in MD snapshots if its distance d_{ij} is <0.65 nm. A salt bridge (SB) between two charged residues was considered formed if the distance between two specific atoms remains within 4.6 Å.

Secondary Structure. To estimate the secondary structures of all peptides, we used the STRIDE algorithm.[77] The percentage of β-strands in the solid-state NMR $A\beta_{40}$ and $A\beta_{42}$ fibrils is 57% (spanning residues 10−23 and 30−38) and 45% (spanning residues 18−26 and 31−40) using the full amino acid sequences, respectively.

Free Energy Landscape. The free-energy surface (FES) along the N-dimensional reaction coordinated $V = (V_1,...,V_N)$ is given by $\Delta G(V) = -k_B T[\ln P(V) - \ln P_{max}]$, where $P(V)$ is the probability distribution obtained from a histogram of MD data. P_{max} is the maximum of the distribution, which is subtracted to ensure that $\Delta G = 0$ for the lowest-free-energy minimum. For the monomers, we used dihedral principal component analysis (dPCA).[78] For the dimers, we used the first two principal components obtained from PCA using the inverse distances between the interpeptide side chain contacts. The higher order principal components were neglected as they contain less than 37% information about sampled conformations for all studied systems (results not shown). For detailed characterization of the free energy minima, we calculated several properties using all snapshots belonging to a state, and not just a single representative structure of a state. For the dimers, we also defined a topological descriptor ranging from a two-stranded β-sheet to a four-stranded β-sheet. Here, at least two interpeptide H-bonds must be formed between consecutive β-strands to pass from a n-stranded β-sheet to a n + 1-stranded β-sheet.

The CCS of all dominant monomeric and dimeric structures was also calculated using the MOBCAL software and the trajectory method[50] which treats the molecule as a collection of atoms represented by a 12-6-4 potential, and is often used for proteins.[79]

ASSOCIATED CONTENT

Supporting Information

Table S1 provides the solvation free energy of dimers. Table S2 gives the populations of intermolecular salt-bridges in the dimeric systems. Figure S1 shows the time dependence potential energy of monomeric and dimeric $A\beta_{42}$ systems. Figures S2−S6 represent the time evolution of secondary structures, R_g, and solvent accessible area for various systems. The free energy surface for monomers $A\beta_{40}$-H6R and $A\beta_{42}$-H6R is presented in Figure S7. Figure S8 shows populations of the intermolecular 22−28 and 23−28 salt-bridge distances. The distributions of β-content along residues of the minimum states Si presented on free energy landscapes of the dimer systems are shown in Figures S9 and S10. Figures S11 and S12 show the time dependence of R_g obtained by OPLS and AMBER force fields for dimers. Figures S13 and S14 show per-residue distributions of dimer secondary structures obtained by OPLS and AMBER force fields in five 100 ns MD runs starting from dominant structures. This material is available free of charge via the Internet at http://pubs.acs.org.

AUTHOR INFORMATION

Corresponding Authors

*E-mail: mhviet@ifpan.edu.pl.
*E-mail: nguyen@ibpc.fr.
*E-mail: derreuma@ibpc.fr.
*E-mail: masli@ifpan.edu.pl.

Author Contributions

M.H.V. and P.H.N. performed MD simulations. All authors analyzed the data. M.S.L. and P.D. wrote the manuscript.

Funding

The work was supported by Narodowe Centrum Nauki in Poland (Grant No. 2011/01/B/NZ1/01622) and Department of Science and Technology at Ho Chi Minh city, Vietnam. P.D. also acknowledges support from the ANR 12-BS07-0017-01. P.D. and M.S.L. also acknowledge funding from a Cooperation between CNRS (France) and Polish Academy of Sciences (Poland) for 2013−2014.

Notes

The authors declare no competing financial interest.

■ ACKNOWLEDGMENTS

Allocation of CPU time at the supercomputer center TASK in Gdansk (Poland) is highly appreciated.

■ REFERENCES

(1) Henderson, A. S., and Jorm, A. F. (2002) *Dementia*, Chapter 1, John Wiley & Sons Ltd., New York.

(2) Hardy, J., and Selkoe, D. J. (2002) Medicine - The amyloid hypothesis of Alzheimer's disease: Progress and problems on the road to therapeutics. *Science 297*, 353−356.

(3) Citron, M. (2004) Strategies for disease modification in Alzheimer's disease. *Nat. Rev. Neurosci. 5*, 677−685.

(4) Aguzzi, A., and O'Connor, T. (2010) Protein aggregation diseases: pathogenicity and therapeutic perspectives. *Nat. Rev. Drug Discovery 9*, 237−248.

(5) Lue, L. F., Kou, Y. M., and Roher, A. E. (1999) Soluble amyloid β peptide concentration as a predictor of synaptic change in Alzheimer's disease. *Am. J. Pathol. 155*, 853−862.

(6) Querfurth, H. W., and Laferla, F. M. (2010) Mechanisms of disease Alzheimer's disease. *N. Engl. J. Med. 362*, 329−344.

(7) Cummings, J. L. (2004) Alzheimer's Disease. *N. Engl. J. Med. 351*, 56−67.

(8) Kayed, R., Head, E., Thompson, J. L., McIntire, T. M., Milton, S. C., Cotman, C. W., and Glabe, C. G. (2003) Common structure of soluble amyloid oligomers implies common mechanism of pathogenesis. *Science 300*, 486−489.

(9) Caughey, B., and Lansbury, P. T. (2003) Protofibrils, pores, fibrils, and neurodegeneration: Separating the responsible protein aggregates from the innocent bystanders. *Annu. Rev. Neurosci. 26*, 267−298.

(10) Walsh, D. M., and Selkoe, D. J. (2007) Aβ oligomers - a decade of discovery. *J. Neurochem. 101*, 1172−1184.

(11) Chebaro, Y., and Derreumaux, P. (2009) Targeting the early steps of Aβ16−22 protofibril disassembly by N-methylated inhibitors: A numerical study. *Proteins 75*, 442−452.

(12) Anand, P., Nandel, F. S., and Hansmann, U. H. E. (2008) The Alzheimer beta-amyloid (A beta(1−39)) dimer in an implicit solvent. *J. Chem. Phys. 129*, 195102.

(13) Berhanu, W. M., and Hansmann, U. H. E. (2012) Structure and dynamics of amyloid-beta segmental polymorphisms. *PLoS One 7*, e41479.

(14) Wu, C., Bowers, M. T., and Shea, J. E. (2010) Molecular structures of quiescently grown and brain-derived polymorphic fibrils of the Alzheimer amyloid A beta(9−40) peptide: A comparison to agitated fibrils. *PloS Comput. Biol. 6*, e1000693.

(15) Bernstein, S. L., Dupuis, N. F., Lazo, N. D., Wyttenbach, T., Condron, M. M., Bitan, G., Teplow, D. B., Shea, J. E., Ruotolo, B. T., Robinson, C. V., and Bowers, M. T. (2009) Amyloid-beta protein oligomerization and the importance of tetramers and dodecamers in the aetiology of Alzheimer's disease. *Nat. Chem. 1*, 326−331.

(16) Hendriks, L., van Duijin, C. M., Cras, P., Cruts, M., Hul, W. V., van Harskamp, F., Warren, A., McInnis, M. G., Antoarakis, S. E., Martin, J.-J., Hofman, A., and Broekhoven, C. V. (1992) Presenil dementia and cerebral haemorrhage linked to a mutation at codon 692 of the β-amyloid precursor protein gene. *Nat. Genet. 1*, 218−221.

(17) Levy, E., Carman, M. D., Fernandez-Madrid, I. J., Power, M. D., Lieberburg, I., van Duinen, S. G., Bots, G. T. A. M., Luyendijk, W., and Frangione, B. (1990) Mutation of the Alzheimer's disease amyloid gene in hereditary cerebral hemorrhage, Dutch type. *Science 1*, 1124−1126.

(18) Bugiani, O., Padovani, A., Magoni, M., Andora, G., Sgarzi, M., Savoiardo, M., Bizzi, A., Giaccone, G., Rossi, G., and Tagliavini, F. (1998) An Italian type of HCHWA. *Neurobiol. Aging 19*, S238.

(19) Kamino, K., et al. (1992) Linkage and mutational analysis of familial Alzheimer disease kindreds for the APP gene region. *Am. J. Hum. Genet. 51*, 998−1014.

(20) Grabowski, T. J., Cho, H. S., Vonsattel, J. P., Rebeck, G. W., and Greenberg, S. M. (2001) Novel amyloid precursor protein mutation in an Iowa family with dementia and severe cerebral amyloid angiopathy. *Ann. Nerol. 49*, 697−705.

(21) Tomiyama, T., Nagata, T., Shimada, H., Teraoka, R., Fukushima, A., Kanemitsu, H., Takuma, H., Kuwano, R., Imagawa, M., Ataka, S., Wada, Y., Yoshioka, E., Nishizaki, T., Watanabe, Y., and Mori, H. (2008) A new amyloid beta variant favoring oligomerization in Alzheimer's-type dementia. *Ann. Neurol. 63*, 377−387.

(22) Massi, F., and Straub, J. E. (2001) Probing the origins of increased activity of the E22Q "Dutch" mutant Alzheimer's beta-amyloid peptide. *Biophys. J. 81*, 697−709.

(23) Cote, S., Derreumaux, P., and Mousseau, N. (2011) Distinct morphologies for amyloid beta protein monomer: Aβ_{1-40}, Aβ_{1-42}, and Aβ_{1-40}(D23N). *J. Chem. Theor. Comp 7*, 2584−2592.

(24) Lin, Y.-S., and Pande, V. S. (2012) Effects of familial mutations on the monomer structure of Aβ_{42}. *Biophys. J. 103*, L47−L49.

(25) Huet, A., and Derreumaux, P. (2006) Impact of the mutation A21G (Flemish variant) on Alzheimer's β-amyloid dimers by molecular dynamics simulations. *Biophys. J. 91*, 3829−3840.

(26) Coskuner, O., Wise-Scira, O., Perry, G., and Kitahara, T. (2013) The structures of the E22Δ mutant-type amyloid-β alloforms and the impact of E22Δ mutation on the structures of the wild-type amyloid-β alloforms. *ACS Chem. Neurosci. 4*, 310−320.

(27) Mitternacht, S., Staneva, I., Hard, T., and Irback, A. (2010) Comparing the folding free-energy landscapes of Aβ42 variants with different aggregation properties. *Proteins 78*, 2600−2608.

(28) Mitternacht, S., Staneva, I., Hard, T., and Irback, A. (2011) Monte Carlo study of the formation and conformational properties of dimers of A beta 42 variants. *J. Mol. Biol. 410*, 357−367.

(29) Petkova, A. T., Yau, W. M., and Tycko, R. (2006) Experimental constraints on quaternary structure in Alzheimer's β-amyloid Fibrils. *Biochemistry 45*, 498−512.

(30) Paravastu, A. K., Leapman, R. D., Yau, W. M., and Tycko, R. (2008) Molecular structural basis for polymorphism in Alzheimer's β-amyloid fibrils. *Proc. Natl. Acad. Sci. U.S.A. 105*, 18349−18354.

(31) Luhrs, T., Ritter, C., Adrian, M., Riek-Loher, D., Bohrmann, B., Doeli, H., Schubert, D., and Riek, R. (2005) 3D structure of Alzheimer's amyloid-β(1−42) fibrils. *Proc. Natl. Acad. Sci. U.S.A. 102*, 17342−17347.

(32) Bertini, I., Gonnelli, L., Luchinat, C., Mao, J. F., and Nesi, A. (2011) A new structural model of A beta(40) fibrils. *J. Am. Chem. Soc. 133*, 16013−16022.

(33) Scheidt, H. A., Morgado, I., Rothemund, S., and Huster, D. (2012) Dynamics of amyloid beta fibrils revealed by solid-state NMR. *J. Biol. Chem. 287*, 2017−2021.

(34) Lu, J. X., Qiang, W., Yau, W. M., Schwieters, C. D., Meredith, S. C., and Tycko, R. (2013) Molecular structure of beta-amyloid fibrils in Alzheimer's disease brain tissue. *Cell 154*, 1257−1268.

(35) Janssen, J. C., Beck, J. A., Campbell, T. A., Dickinson, A., Fox, N. C., Harvey, R. J., Houlden, H., Rossor, M. N., and Collinge, J. (2003) Early onset familial Alzheimer's disease: Mutation frequency in 31 families. *Neurology 60*, 235−239.

(36) Hori, Y., Hashimoto, T., Wakutani, Y., Urakami, K., Nakashima, K., Condron, M. M., Tsubuki, S., Saido, T. C., Teplow, D. B., and Iwatsubo, T. (2007) The Tottori (D7N) and English (H6R) familial Alzheimer Disease mutations accelerate Aβ fibril formation without inscreasing protofibril formation. *J. Biol. Chem. 282*, 4916−4923.

(37) Chen, W. T., Hong, C. J., Lin, Y. T., Chang, W. H., Huang, H. T., Liao, J. Y., Chang, Y. J., Hsieh, Y. F., Cheng, C. Y., Liu, H. C., Chen, Y. R., and Cheng, I. H. (2012) Amyloid-beta (Aβ) D7H mutation increases oligomeric Aβ42 and alters properties of Aβ-Zinc/Copper assemblies. *PLoS One 7*, e35807.
(38) Wakutani, Y., Watanabe, K., Adachi, Y., Wada-Isoe, K., Urakami, K., Ninomiya, H., Saido, T. C., Hashimoto, T., Iwatsubo, I., and Nakashima, K. (2004) Novel amyloid precursor protein gene missense mutation (D678N) in probable familial Alzheimer's disease. *J. Neurol., Neurosurg. Psychiatry 75*, 1039−1042.
(39) Ono, K., Condron, M. M., and Teplow, D. B. (2010) Effects of the English (H6R) and Tottori (D7N) familial Alzheimer disease mutations on amyloid beta-protein assembly and toxicity. *J. Biol. Chem. 285*, 23186−23197.
(40) Fede, G. D., Catania, M., Morbin, M., Rossi, G., Suardi, S., Mazzoleni, G., Merlin, M., Giovagnoli, A. R., Prioni, S., Erbetta, A., Falcone, C., Gobbi, M., Colombo, L., Bastone, A., Beeg, M., Manzoni, C., Francescucci, B., Spagnoli, A., Cantù, L., Favero, E. D., Levy, E., Salmona, M., and Tagliavini, F. (2009) Recessive Mutation in the APP Gene with Dominant-Negative Effect on Amyloidogenesis. *Science 323*, 1473−1477.
(41) Lv, Z. J., Roychaudhuri, R., Condron, M. M., Teplow, D. B., and Lyubchenko, Y. L. (2013) Mechanism of amyloid beta-protein dimerization determined using single-molecule AFM force spectroscopy. *Sci. Rep. 3*, srep02880.
(42) Nguyen, P. H., Tarus, B., and Derreumaux, P. (2013) Familial Alzheimer A2V Mutation Reduces the Intrinsic Disorder and Completely Changes the Free Energy Landscape of the Aβ_{1-28} Monomer. *J. Phys. Chem. B 118*, 501−510.
(43) Viet, M. H., Nguyen, P. H., Ngo, S. T., Li, M. S., and Derreumaux, P. (2013) Effect of the Tottori Familial Disease Mutation (D7N) on the Monomers and Dimers of Aβ40 and Aβ42. *ACS Chem. Neurosci. 4*, 1446−1457.
(44) Reddy, G., Straub, J. E., and Thirumalai, D. (2009) Influence of preformed Asp23-Lys28 salt bridge on the conformational fluctuations of monomers and dimers of Aβ peptides with implications for rates of fibril formation. *J. Phys. Chem. B 113*, 1162−1172.
(45) Li, M. S., Co, N. T., Hu, C. K., Straub, J. E., and Thirumalai, D. (2010) Determination of factors governing fibrillogenesis of polypeptide chains using lattice models. *Phys. Rev. Lett. 105*, 218101.
(46) Sciarretta, K. L., Gordon, D. J., Petkova, A. T., Tycko, R., and Meredith, S. C. (2005) Aβ40-Lactam(D23/K28) models a conformation highly favorable for nucleation of amyloid. *Biochemistry 44*, 6003−6014.
(47) Bellesia, G., and Shea, J.-E. (2009) Effect of β-sheet propensity on peptide aggregation. *J. Chem. Phys. 130*, 145103.
(48) Nam, H. B., Kouza, M., Zung, H., and Li, M. S. (2010) Relationship between population of the fibril-prone conformation in the monomeric state and oligomer formation times of peptides: Insights from all-atom simulations. *J. Chem. Phys. 132*, 165104.
(49) Gessel, M. M., Bernstein, S., Kemper, M., Teplow, D. B., and Bowers, M. T. (2012) Familial Alzheimer's Disease mutations differentially alter amyloid β-protein oligomerization. *ACS Chem. Neurosci. 3*, 909−918.
(50) Mesleh, M. F., Hunter, J. M., Shvartsburg, A. A., Schatz, G. C., and Jarrold, M. F. (1996) Structural information from ion mobility measurements: Effects of the long range potential. *J. Phys. Chem. 100*, 16082.
(51) Baumketner, A., Bernstein, S. L., Wyttenbach, T., Bitan, G., Teplow, D. B., Bowers, M. T., and Shea, J. E. (2006) Amyloid β-protein monomer structure: A computational and experimental study. *Protein Sci. 15*, 420−428.
(52) Kollman, P., Massova, I., Reyes, C., Kuhn, B., Huo, S., Chong, L., Lee, M., Lee, T., Duan, Y., Wang, W., Donini, O., Cieplak, P., Srinivasan, J., Case, D., and T.E. Cheatham, I. (2000) Calculating structures and free energies of complex molecules: combining molecular mechanics and continuum models. *Acc. Chem. Res. 33*, 889−897.
(53) Nguyen, T. T., Mai, B. K., and Li, M. S. (2011) Study of tamiflu sensitivity to variants of A/H5N1 virus using different force fields. *J. Chem. Inf. Model. 51*, 2266−2276.
(54) Viet, M. H., and Li, M. S. (2012) Amyloid peptide Aβ_{40} inhibits aggregation of Aβ_{42}: Evidence from molecular dynamics simulations. *J. Chem. Phys. 136*, 245105.
(55) Sharp, K. A., and Honig, B. (1990) Electrostatic interactions in macromolecules: theory and applications. Annu. Rev. Biophys. *Biophys. Chem. 19*, 301−332.
(56) Baker, N. A., Sept, D., Joseph, S., Holst, M. J., and McCammon, J. A. (2001) Electrostatics of nanosystems: application to microtubules and the ribosome. *Proc. Natl. Acad. Sci. U.S.A. 98*, 10037−10041.
(57) Shrake, A., and Rupley, J. A. (1973) Environment and exposure to solvent of protein atoms-lysozyme and insulin. *J. Mol. Biol. 79*, 351−371.
(58) Sitkoff, D., Sharp, K. A., and Honig, B. (1994) Accurate calculation of hydration free energies using macroscopic solvent models. *J. Phys. Chem. 97*, 1978−1988.
(59) Maji, S. K., Loo, R. R. O., Inayathullah, M., Spring, S. M., Vollers, S. S., Condron, M. M., Bitan, G., Loo, J. A., and Teplow, D. B. (2009) Amino Acid Position-specific Contributions to Amyloid beta-Protein Oligomerization. *J. Biol. Chem. 284*, 23580−23591.
(60) Hornak, V., Abel, R., Okur, A., Strockbine, B., Roitberg, A., and Simmerling, C. (2006) Comparison of Multiple Amber Force Fields and Development of Improved Protein Backbone Parameters. *Proteins: Struct., Funct., Bioinf. 65*, 712−725.
(61) Jorgensen, J. W., Chandrasekhar, J., Madura, J. D., Imprey, R. W., and Klein, M. L. (1983) Comparison of simple potential functions for simulating liquid water. *J. Chem. Phys. 79*, 926.
(62) van Gunsteren, W. F., Billeter, S. R., Eising, A. A., Hunenberger, P. H., Kruger, P., Mark, A. E., Scott, W. R. P., and Tironi, I. G. (1996) *Biomolecular Simulation: The GROMOS96 Manual and User Guide*, Vdf Hochschulverlag AG an der ETH Zurich, Zurich.
(63) Nguyen, T. T., Viet, M. H., and Li, M. S. (2014) Effects of water models on binding affinity: Evidence from all-atom simulation of binding of tamiflu to A/H5N1 neuraminidase. *Sci. World J. 2014*, 536084.
(64) Coles, M., Bicknell, W., Watson, A. A., Fairlie, D. P., and Craik, D. J. (1998) Solution structure of amyloid beta-peptide(1−40) in a water-micelle environment. Is the membrane-spanning domain where we think it is? *Biochemistry 37*, 11064−11077.
(65) Tomaselli, S., Esposito, V., Vangone, P., van Nuland, N. A., Bonvin, A. M., Guerrini, R., Tancredi, T., Temussi, P. A., and Picone, D. (2006) The α-to-β conformational transition of Alzheimer's Aβ-(1−42) peptide in aqueous media is reversible: a step by step conformational analysis suggests the location of β conformation seeding. *ChemBioChem 7*, 257−267.
(66) Kaminski, G. A., and Friesner, R. A. (2001) Evaluation and reparametrization of the OPSL-AA force field for proteins via comparison with accurate quantum chemical calculations on peptides. *J. Phys. Chem. B 105*, 6474−6487.
(67) Jorgensen, W. L., and Madura, J. D. (1985) *Mol. Phys. 56*, 1381−1392.
(68) *PyMOL: The PyMOL Molecular Graphics System*, Version 1.3, Schrodinger, LLC.
(69) Hess, B., Kutzner, C., van der Spoel, D., and Lindahl, E. (2008) GROMACS 4: Algorithms for highly efficient, load-balanced, and scalable molecular simulation. *J. Chem. Theory Comput. 4*, 435−447.
(70) Sgourakis, N. G., Yan, Y. L., McCallum, S. A., Wang, C. Y., and Garcia, A. E. (2007) The Alzheimer's peptides Aβ40 and 42 adopt distinct conformations in water: A combined MD/NMR study. *J. Mol. Biol. 368*, 1448−1457.
(71) Nguyen, P. H., Derreumaux, P., and Li, M. S. (2011) Effects of all-atom force fields on amyloid oligomerization: Replica exchange molecular dynamics simulations of the Aβ_{16-22} dimer and trimer. *Phys. Chem. Chem. Phys. 13*, 9778.
(72) Hockney, R. W., Goel, S. P., and Eastwood, J. (1974) Quit high resolution computer models of plasma. *J. Comput. Phys. 14*, 148−158.

(73) Hess, B., Bekker, H., Berendsen, H. J. C., and Fraaije, J. G. E. M. (1997) LINCS: A linear constraint solver for molecular simulations. *J. Comput. Chem. 18*, 1463−1472.
(74) Bussi, G., Donadio, D., and Parrinello, M. (2007) Canonical sampling through velocity rescaling. *J. Chem. Phys. 126*, 014101.
(75) Berendsen, H. J. C., Postma, J. P. M., Vangunsteren, W. F., Dinola, A., and Haak, J. R. (1984) Molecular-dynamics with coupling to an external bath. *J. Chem. Phys. 81*, 3684−3690.
(76) Darden, T., York, D., and Pedersen, L. (1993) Particle mesh Ewald: An Nlog(N) method for Ewald sums in large systems. *J. Chem. Phys. 98*, 10089−10092.
(77) Heinig, M., and Frishman, D. (2004) STRIDE: a Web server for secondary structure assignment from known atomic coordinates of proteins. *Nucleic Acids Res. 32*, W500-2.
(78) Mu, Y., Nguyen, P. H., and Stock, G. (2005) Energy landscape of a small peptide revealed by dihedral angle principal component analysis. *Proteins 58*, 45−52.
(79) Chong, S.-H., and Ham, S. (2012) Atomic-level investigations on the amyloid-β dimerization process and its driving forces in water. *Phys. Chem. Chem. Phys. 14*, 1573−1575.